

Rotation of young stars in Cepheus OB3b

S. P. Littlefair,^{1*} Tim Naylor,² N. J. Mayne,² Eric S. Saunders³ and R. D. Jeffries⁴

¹*Department of Physics and Astronomy, University of Sheffield, S3 7RH*

²*School of Physics, University of Exeter, Exeter EX4 4QL*

³*Las Cumbres Observatory, 6740 Cortona Dr, Suite 102, Santa Barbara, CA 93117, USA*

⁴*School of Chemistry and Physics, Keele University, Keele, Staffordshire ST5 5BG*

Accepted 2009 November 17. Received 2009 November 17; in original form 2009 October 7

ABSTRACT

We present a photometric study of *I*-band variability in the young association Cepheus OB3b. The study is sensitive to periodic variability on time-scales of less than a day, to more than 20 d. After rejection of contaminating objects using *V*, *I*, *R* and narrow-band $H\alpha$ photometry, we find 475 objects with measured rotation periods, which are very likely pre-main-sequence members of the Cep OB3b star-forming region.

We revise the distance and age to Cep OB3b, putting it on the self-consistent age and distance ladder of Mayne & Naylor. This yields a distance modulus of 8.8 ± 0.2 mag, corresponding to a distance of 580 ± 60 pc, and an age of 4–5 Myr.

The rotation period distribution confirms the general picture of rotational evolution in young stars, exhibiting both the correlation between accretion (determined in this case through narrow-band $H\alpha$ photometry) and rotation expected from disc locking, and the dependence of rotation upon mass that is seen in other star-forming regions. However, this mass dependence is much weaker in our data than found in other studies. Comparison to the similarly aged NGC 2362 shows that the low-mass stars in Cep OB3b are rotating much more slowly. This points to a possible link between star-forming environment and rotation properties. Such a link would call into question models of stellar angular momentum evolution, which assume that the rotational period distributions of young clusters and associations can be assembled into an evolutionary sequence, thus ignoring environmental effects.

Key words: accretion, accretion discs – planetary systems: protoplanetary discs – stars: pre-main-sequence.

1 INTRODUCTION

There are sound theoretical reasons to expect that accretion processes help determine the angular momentum of T-Tauri stars. Historically, the slow rotation rates of T Tauri stars (relative to their break-up velocity) have been explained by the disc-locking theory (Koenigl 1991; Shu et al. 1994). In this theory, magnetic field lines connect the star to the disc, enforcing synchronous rotation between the star and the material in the disc at some radius, near where the magnetic field disrupts the disc. The simplistic theory has been expanded in a variety of models where angular momentum is removed from the star by a combination of the disc and an accretion-driven wind (e.g. Fendt 2007; Romanova, Kulkarni & Lovelace 2007; Matt & Pudritz 2008). Whether the star is spun up or down by the star-disc interaction depends upon the balance between accretion spinning up the star and magnetic (or wind) torques

slowing it down. Theoretically, this issue is unresolved; some studies find the star spins up (Bessolaz et al. 2008), some find it spins down (e.g. Long, Romanova & Lovelace 2005).

Observationally, the evidence for the influence of accretion disks on rotation is much stronger than it was a few years ago (Herbst et al. 2007). Previously, conflicting results had arisen (e.g. Stassun et al. 1999; Herbst et al. 2002; Littlefair et al. 2005). These were most likely due to a combination of small sample sizes, and ambiguous diagnostics of the presence of accretion discs. Rebull et al. (2005) resolved these issues with a large sample of rotation periods in the Orion Nebula Cluster (ONC), and accretion disc status defined from *Spitzer* *IRAC* data. Rebull et al. (2005) found a clear correlation between mid-infrared (mid-IR) excess and rotation, in the sense that stars with mid-IR excess were much more likely to be slow rotators. An analysis of the slightly older NGC 2264 found the same result (Cieza & Baliber 2007), and confirmed the Rebull et al. (2005) result, via a refined analysis of the same data. There is thus strong observational evidence that the star-disc interaction is responsible for extracting angular momentum from young stars. Interestingly,

*E-mail: s.littlefair@shef.ac.uk

a small population of rapidly rotating stars with mid-IR excesses exists; it is possible that these stars are being spun-up by accretion, hinting that the braking process of young stars is intermittent. Also, in both the ONC and NGC 2264, there exists a significant population of slow rotators with *no* mid-IR excess. These are often interpreted as being recently released from disc-locking, but there are problems with this interpretation (see Bouvier et al. 2007, for example).

The firm link established between accretion and rotation represents significant progress, but there are still open questions regarding the rotation of young stars. For example, the low-mass stars are rotating more rapidly than the high-mass stars, and appear to spin-up more rapidly as they contract towards the main sequence (Herbst et al. 2002; Irwin et al. 2007). The reason for this is still not known. Also, the angular momentum evolution of young stars is determined by assembling different clusters into an evolutionary sequence, and assuming the period distribution of the older clusters can be modelled using the young clusters as a starting point. In doing so, the possibility of an environmental effect on rotation is ignored. Such an environmental effect may be indicated by the data; the young stars in IC348 rotate much slower than those in the similarly aged NGC 2264 (Littlefair et al. 2005).

Here, we present a photometric study of the young association Cepheus OB3b (Cep OB3b). Cep OB3 is a young association covering a region of the sky from approximately $22^{\text{h}}46^{\text{m}}$ to $23^{\text{h}}10^{\text{m}}$ in right ascension and $+61^{\circ}$ to $+64^{\circ}$ in declination. The subgroup Cep OB3b lies closest to the molecular cloud, and has a rich pre-main-sequence (PMS) population, confirmed by both spectroscopy (Pozzo et al. 2003) and X-ray data (Getman et al. 2006). In Section 2, we present the observations and data reduction techniques applied. Section 3 describes the techniques used to identify periodic variables. Section 4 provides a revision of the age of, and distance to, Cep OB3b. In Sections 5 and 6, we present our results and analysis of the data, whilst in Section 7 we draw our conclusions.

2 OBSERVATIONS AND DATA REDUCTION

2.1 Observations

I-band CCD images were taken with the Wide Field Camera (WFC) on the Isaac Newton Telescope (INT) on La Palma, equipped with four thinned EEV $2\text{k}\times 4\text{k}$ CCDs. The total sky coverage per exposure is 0.29 deg^2 . A single field, with the centre of CCD No. 4 pointing at $\alpha = 22^{\text{h}}55^{\text{m}}43^{\text{s}}.3$, $\delta = +62^{\circ}40^{\text{m}}13^{\text{s}}$ J2000, was observed, with data being taken on every night between 2004 September 21 and October 6. This data set will be referred to as the ‘short baseline’ (SB) data set. Because the SB data set is not sensitive to periods longer than 7–10 d, we augmented it with two additional data sets, both of which have longer baselines, but less dense sampling. Additional data were taken with the WFC on 29 nights between 2005 August 23 and November 1. This data set is referred to as the ‘long baseline 0’ (LB0) data set.

For the SB data set the seeing varied between 0.8 and 5 arcsec, with a median and standard deviation of 1.1 and 0.9 arcsec, respectively. Most nights were affected by thin to heavy cirrus cloud, although the nights between 2004 September 26 and 29, and the night of 2004 October 5 were photometric. The LB0 data set was taken in seeing conditions between 0.8 and 2.6 arcsec, with a median and standard deviation of 0.9 and 0.8 arcsec, respectively. Most nights were affected by light cirrus only, with less than half of a magnitude effect on transparency. To increase the dynamic range of the SB and LB0 data sets, we used exposure times of 5, 30 and 300 s.

For the SB data set, these were repeated many times throughout a night; for the LB0 data set, one or two exposures were taken each night. In total the SB data set contains 477 useable short exposures, 617 useable medium exposures and 614 useable long exposures. The LB0 data set contains 41 useable short exposures, 41 useable medium exposures and 36 useable long exposures.

The second long-baseline data set consists of Sloan Digital Sky Survey *i'*-band CCD images obtained with DillCam on the 2-m Faulkes Telescope N (FTN). DillCam has a single CCD with a pixel scale of $0.278\text{ arcsec pixel}^{-1}$ in the default 2×2 binning mode, giving a $4.7\times 4.7\text{ arcmin}^2$ field of view. Four fields were observed, chosen to cover the positions of highest stellar density. Data were taken on 15 nights between 2005 October 13 and December 17, with between two and four separate observations per night. Exposure times of 30 and 300 s were used. The number of exposures varies from field to field, and is different for the short and long exposure times, but ranges from 43 to 60 exposures in total. This data set is referred to as the ‘long baseline 1’ (LB1) data set. The LB1 data set was taken in seeing conditions between 1.0 and 3.1 arcsec, with a median and standard deviation of 1.3 and 0.6 arcsec, respectively. The data are only marginally affected by cloud, with transparency variations always less than 0.3 mag.

A plot of the Cep OB3 region and the fields observed is shown in Fig. 1.

Over the nights of 2003 September 12–14, we used the INT to obtain three sets of images of the same field as is covered by our *I*-band data, each set consisting of a 300 s and a 30 s exposure in *H α* and a 30 s and a 3 s exposure in *R*. We debiased and flat-fielded the images in a similar manner to the *I*-band data, but then instead of searching for stars in a combined image, we carried out optimal photometry at the positions of all the objects in the catalogue of Mayne et al. (2007). See Section 2.2 for a complete description of how the photometry was carried out. We then combined the magnitudes from each image, as described in Mayne et al. (2007), to obtain *R* and *R* – *H α* magnitudes, with an arbitrary zero-point. We then combined this with the *V* and *I* photometry of Mayne et al. (2007) to create Table 1 (the full version of which is available electronically).

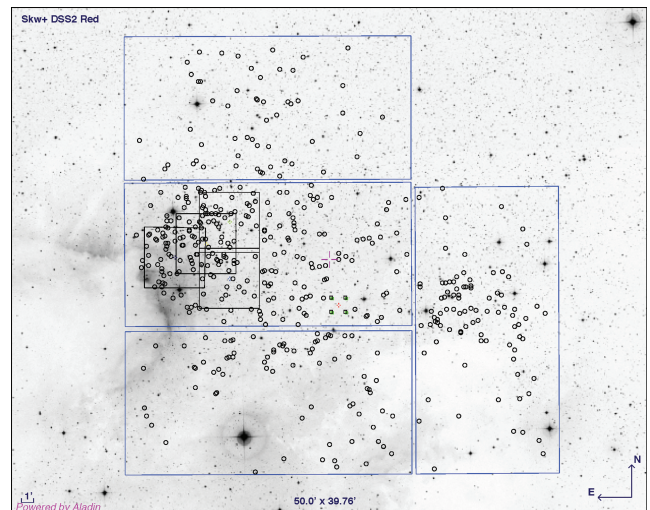


Figure 1. INT WFC field-of-view overlaid on Digitized Sky Survey red image of Cep OB3. Also shown are the four Faulkes telescope pointings obtained. Circles denote the locations of periodic association members (see Section 3 for details).

Table 1. Photometry for the INT WFC field observed is available in this format at <http://www.astro.ex.ac.uk/people/timn/Catalogues/tables.html>. This table is a sample only, to indicate the format of the online table (see also Supporting Information). The flag column indicates data quality, and is explained in full at <http://www.astro.ex.ac.uk/people/timn/Catalogues/format.html>

Field/CCD (field.ccd)	ID	RA (J2000)	Dec. (J2000)	xpos (ccd)	ypos (ccd)	Mag	Uncertainty	Flag	COL	Uncertainty	Flag
1.02	410	22 52 47.929	+62 30 57.08	613.729	2634.474	11.723	0.010	OO	0.763	0.014	OO
1.04	10	22 57 13.885	+62 41 35.55	774.439	119.826	11.596	0.010	OO	0.589	0.013	OO

2.2 Image processing and optimal photometry

Image processing and data reduction were performed in a consistent manner for all data sets. The individual frames were bias subtracted using a median stack of several bias frames. The frames were then flat fielded using twilight sky flats taken on one of the photometric nights. Only sky flats with peak counts of less than 30 000 were used, to avoid non-linearity effects. A bad pixel mask was constructed for all frames by flagging all pixels which deviated by more than 10σ from the median of a ratio of two flat-fields. In addition, a smoothed version of a long exposure was subtracted from the long exposure, and all pixels with a value lower than 1000 were masked. These procedures accounted for most bad pixels, but left a number of bad columns unmasked. These columns were identified by hand and added to the bad pixel mask.

The processed CCD frames were then analysed using optimal photometry, as implemented by the `CLUSTER` software described in detail by Naylor et al. (2002), with modifications described by Littlefair et al. (2005). Advantages of this approach over classical aperture photometry include better signal-to-noise ratios (S/N), and robustly determined uncertainties for each observation. Photometric measurements which are deemed of poor quality are flagged rather than rejected. The reduction of our data sets closely follows that of Littlefair et al. (2005). Profile corrections (analogous to aperture corrections in classical aperture photometry) were allowed to vary as a second order polynomial function of position upon the CCD.

After profile correction, the photometric measurements were adjusted for any difference in the airmass and transparency for each frame, by determining a relative transparency correction from the bright stars. Before this process we added an additional, magnitude-independent error of 0.01 mag to the results of each frame, in order to yield a plot of χ^2_v versus S/N that was flat and had a modal value of approximately 1. In the absence of colour information, transparency correction may introduce errors into our relative photometry because of the colour dependence of extinction. Following the analysis of Littlefair et al. (2005), we find that any errors introduced should be smaller than 3 mmag. Hence, we are confident that this effect is negligible for the purpose of our analysis. An astrometric solution was achieved through comparison with a Two-Micron All-Sky Survey catalogue of the same region. A six-coefficient solution to yield an rms discrepancy in positions which was always less than 0.14 arcsec.

2.3 Transformation to a standard system

Our aim for this data set was to obtain high-standard relative photometry of Cep OB3b. This meant that we did not measure colour information for each star at each epoch, and hence we are unable to tie our photometry to a standard system directly. Instead, we use the *BVI* photometry of Mayne et al. (2007) throughout this paper.

2.4 Final data set

The final data set consists of light curves for 42 962 stars. Rather than combine data with very different sizes of error bars, three light curves were produced for each star, resulting from the 300, 30 and 5 s exposures (where available). This was done for each of the SB, LB0 and LB1 data sets, resulting in a maximum of eight light curves for each star. Fig. 2 shows the rms variability in magnitudes for our stars, plotted as a function of magnitude. This plot shows the high internal accuracy reached in our data set. In both the SB and LB0 data sets, obtained with the INT WFC, the 300 and 30 s data sets have an internal accuracy of better than 1 per cent, whilst the 5 s data set has an internal accuracy of 2 per cent. The gradual decrease in internal accuracy with decreasing exposure time is most likely due to a corresponding decrease in the number of stars available to perform the transparency correction. The LB1 data set, taken on the FTN, reaches an accuracy of 1 per cent in both the 30 and 300 s exposures.

3 DETECTION OF PERIODIC VARIABLES

To search for periodic variables within our data sets, Lomb-Scargle periodograms were calculated independently for each of the SB, LB0 and LB1 data sets. Frequencies corresponding to periods from 0.1 to 12 d were searched for the SB data set, and 4–25 d for the LB0 and LB1 data sets. In each case, the lower value is set by the ‘mean Nyquist’ frequency of the light curve.

Searching for periodicities in photometry of young stars is a challenging task. The unevenly spaced data sampling means that analytical estimates of the false alarm probability (FAP) (e.g. Linnell Nemeč & Nemeč 1985; Horne & Baliunas 1986) are rendered invalid. Worse still, many young stars show irregular variability as well as, or instead of, periodic photometric modulations from surface spots. The interaction of this intrinsic variability with the often patchy sampling window can quite easily introduce peaks into a periodogram which appear significant based on a simple FAP cut.

The inadequacy of analytical estimates of FAP is often sidestepped by estimating the FAP via a Monte Carlo simulation; the FAP is set to be the fraction of simulated light curves where the peak power exceeds the observed peak power. The simulated light curves can either have pure Gaussian noise added or some correlated noise model can be assumed. Eventually, one ends up with a cut-off level for the peak power, above which a period is judged to be significant.

The goal of these Monte Carlo simulations is to estimate the heights of spurious peaks which may arise in the periodogram due to a combination of imperfect sampling, and variability in the light curve. However, they can only realistically account for variability in the light curve due to photometric error. For a large number of young stars, intrinsic variability is larger than the photometric errors. In addition, colour-dependent effects mean that transparency

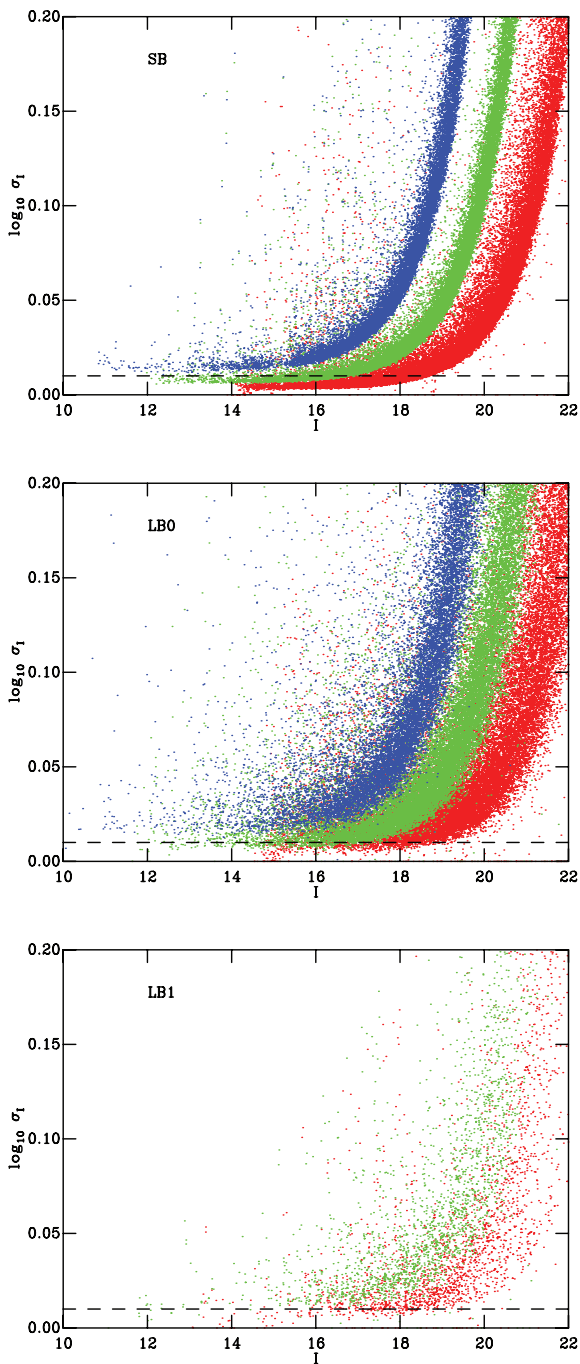


Figure 2. Scatter in the photometry of stars as a function of brightness in the SB (top), LB0 (middle) and LB1 (bottom) data sets. The 300 s exposures are plotted in red (dark grey), the 30 s exposures in green (light grey) and the 5 s exposures in blue (black). The dotted line marks a photometric precision of 1 per cent.

variations can be imperfectly corrected, introducing a night-to-night variability that Monte Carlo simulations do not attempt to account for. Selecting periodic variables solely on the basis of Monte Carlo simulations to assess FAP can thus lead to significant contamination of a data set by spurious periods. The large number of objects with periods very close to 1 d in the NGC 2264 data set of Lamm et al. (2005) and Lamm et al. (2004) may be an example of this.

What we are aiming for is a sample of genuine periodic variables, which is relatively free from contamination by spurious pe-

riods. Since we have a large sample of light curves to search, one approach is to use the light curves themselves as a mean of estimating the height of spurious peaks introduced into the periodogram by all factors affecting the data set, from imperfect photometry to intrinsic variability. We calculate an analytical FAP, as estimated by Horne & Baliunas (1986), FAP_h , for the strongest peak in all our light curves. Assuming that most stars in our field of view are not periodic, the distribution of FAP_h is determined by the interplay of stellar variability, finite S/N and systematic effects in our photometry with the sampling windows of our light curves. Candidate periodic variables can be selected as outliers in the FAP_h distribution. The value of FAP_h to make a cut at is selected from a histogram of the FAP_h values from our light curves. The value of FAP_h is chosen by-eye from the histograms shown in Fig. 3. After applying the additional selection criteria described below, the level of contamination is assessed by visual inspection of randomly selected folded light curves, and the chosen FAP_h value is adjusted to keep the contamination at an acceptable level. During the visual examination of folded light curves, most rejected candidates were those whose periodic nature rested on only a few discrepant points (such as might occur from two flares repeated days apart, for example). Light curves were inspected by a single author (Littlefair), and the process repeated until the results were acceptable. We settled on a FAP_h cut-off of 10^{-35} for the SB data set, and a FAP_h cut-off of 0.005 for the LB0 and LB1 data sets.

A FAP cut taken alone will not reject some objects which should not be included in a sample of periodic variables. Two examples are very irregular variables and stars with poor rotational phase coverage. Repeating patterns in bright, irregular variables can add significant power to a Lomb–Scargle periodogram, and stars with poor phase coverage must necessarily be considered dubious periodic candidates. To remove these interlopers, we applied two further cuts: one on the χ^2_v with respect to a sinusoidal fit at the suggested period, and another on a statistic designed to maximize phase coverage, the S-statistic (Saunders, Naylor & Allan 2006). The S-statistic is the sum of the squares of the phase differences between adjacent data points, after the data have been sorted according to phase. It is normalized by division by the number of data points, such that uniform phase coverage gives an S-statistic of unity, and the S-statistic rises with increasingly irregular phase coverage. The S-statistic is especially good at removing spurious periods arising from the $1-d^{-1}$ natural frequency that is introduced into the data the rotation of the Earth, and observing at a single site. The S-statistic for our data sets as a function of period is shown in Fig. 4. This figure shows the improvements in phase coverage offered by the long baseline data sets; particularly for periods around multiples of a day.¹ We calculate the S-statistic for all the periodic candidates in our sample, after converting to phase using the best-fitting period as deduced from the Lomb–Scargle periodogram. We rejected all stars with an S-statistic greater than 30 (SB), 5 (LB0) and 7 (LB1) or with periods in the ranges 0.9–1.05, 0.495–0.505 and 0.325–0.335 d. The χ^2_v cut was established via a by-eye inspection of 200 randomly

¹ The long-period data sets show spikes in the Saunders statistic at periods between 11 and 15 d. This means the phase coverage of these data sets degrades when the data are folded on these periods. In Fig. 5, we show a graphical representation of the temporal coverage of each of our data sets. Looking at this figure, we can understand that the spikes in Saunders statistic at 11–15 d arise because the long-period data sets have a tendency towards gaps in coverage lasting 5–8 d. We are not able to offer a definitive explanation of the reason for these gaps in coverage, but we can speculate that it is linked to the typical duration of bad weather at our observing sites.

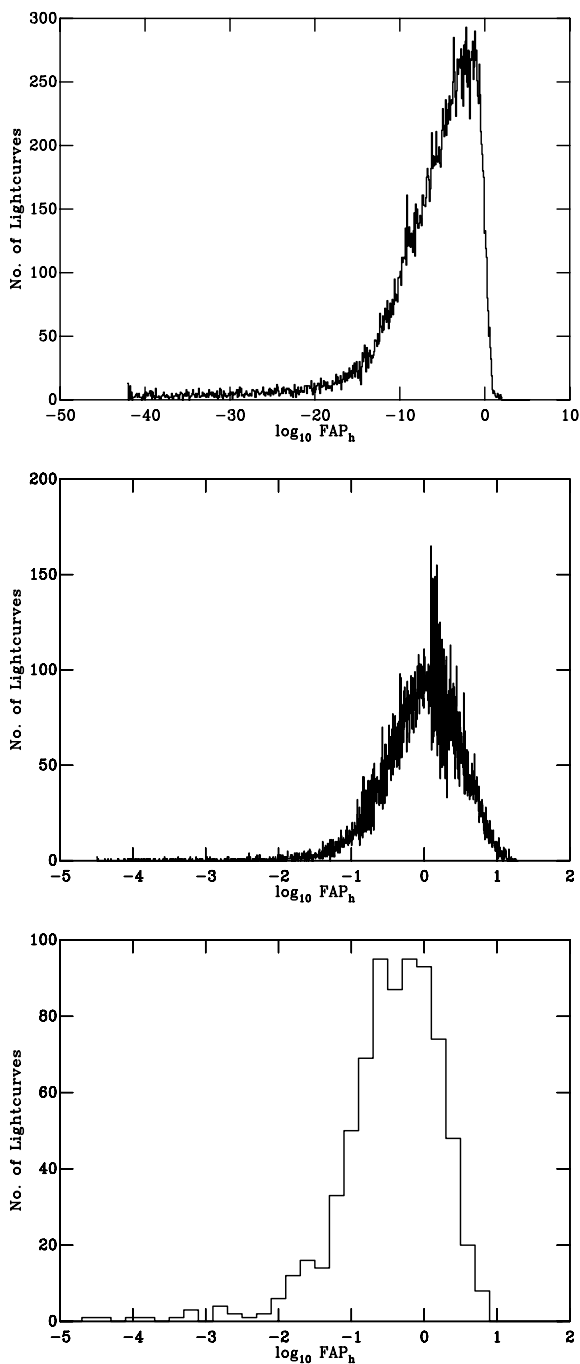


Figure 3. The distribution of FAP_h , for the SB (top), LB0 (middle) and LB1 (bottom) data sets.

selected candidate periodic variables. The value chosen rejected erratic variables, whilst preserving the majority of stars which were clearly periodic, but non-sinusoidal. We are thus confident that the χ^2_v cut is not rejecting periodic variables with a high S/N whose light curves are not purely sinusoidal. All stars with $\chi^2_v > 1.3$ were rejected.

The selection process outlined above is far from perfect, but there is no ideal solution yet found to the problem of searching for periods in an imperfect data set of objects which exhibit significant intrinsic variability. The selection criteria adopted above are conservative; the aim was not to discover all rotational periods, but to produce a catalogue of periodic stars which was relatively free from

the contamination by spurious periods. To check our success in this aim, we undertook a by-eye examination of 200 randomly selected folded light curves. This examination suggests that our final sample of periodic stars has a contamination by spurious periods of ~ 3 per cent.

Once each data set was searched for periods, we combined the results to produce our final catalogue of periodic variables. As each star could have a detected period in each of the data sets, we selected a period from the data set which was most likely to be accurate. For periods longer than 7 d, we adopted a period from the data set with the longest baseline, whilst for shorter periods we adopted a period from the data set with the densest time sampling. Where a data set has light curves with differing exposure times, we always used the deepest light curve in which a period was detected. In the vast majority of cases, periods from different data sets were consistent. Only eight objects showed significant disagreement between data sets; these were long-period systems for which the SB data set lacked sufficient baseline. The final periodic data set consists of 709 periodic variables; 578 from the SB data set, 88 from the LB0 data set and 43 from the LB1 data set. 704 of our periodic variables have *BVI* photometry from Mayne et al. (2007). These 704 objects comprise our final catalogue of periodic variables, and are presented in Table 2, which is available in the online version of this paper.

3.1 Period completeness and selection effects

We investigated our ability to recover a range of periods by introducing artificial sinusoidal signals into our data and checking to see if the correct period was recovered. Light curves from our data sets were selected at random, normalized and had an artificial sinusoidal signal added with a S/N of 2. For our data set, this is equivalent to adding a 0.02-mag signal to an object with $I = 18$ (the faintest magnitude for which report periods, and corresponding roughly to a mass of $0.2 M_{\odot}$). Our simulation is thus directly comparable to the simulation by Irwin et al. (2008) for their periodic data set in NGC 2362. We also performed a simulation in which sinusoidal signals with a S/N of 5 were added to a normalized light curve.

The period-selection process described above was then performed on our artificial light curves. A period was deemed correctly recovered if the recovered period was within 10 per cent of the injected period. Fig. 6 shows the results. The SB data set finds essentially all periods below 7 d, but is incomplete above that. This is expected from the relatively SB of this data set; indeed the reason so few periods are recovered above 10 d is that these periods fail our test based on the Saunders statistic. The LB0 data set improves upon this substantially, but is still not complete above 10 d. Because of the relatively sparse sampling of this data set, completeness for the LB0 data set is a strong function of the injected signal size. For weak signals, the completeness never rises much above 50 per cent, whereas this data set recovers most stronger periodic signals below 10 d. The LB1 data set is largely complete at all periods, with the exception of a small drop in completeness between 12 and 14 d, however, the small spatial coverage of this data set means that it will not be available for many stars.

This simulation shows that all data sets are sensitive to short periods (below 7 d). In practice, the SB data set will be much better at recovering period shorter than 7 d. This is because the simulation described above does not take account of the stochastic variability often seen in young stars. This variability can be considered red noise, and has characteristic time-scales of days to weeks. As discussed by Littlefair et al. (2005), dense sampling of light curves makes it much easier to recover periods in the face of this red noise.

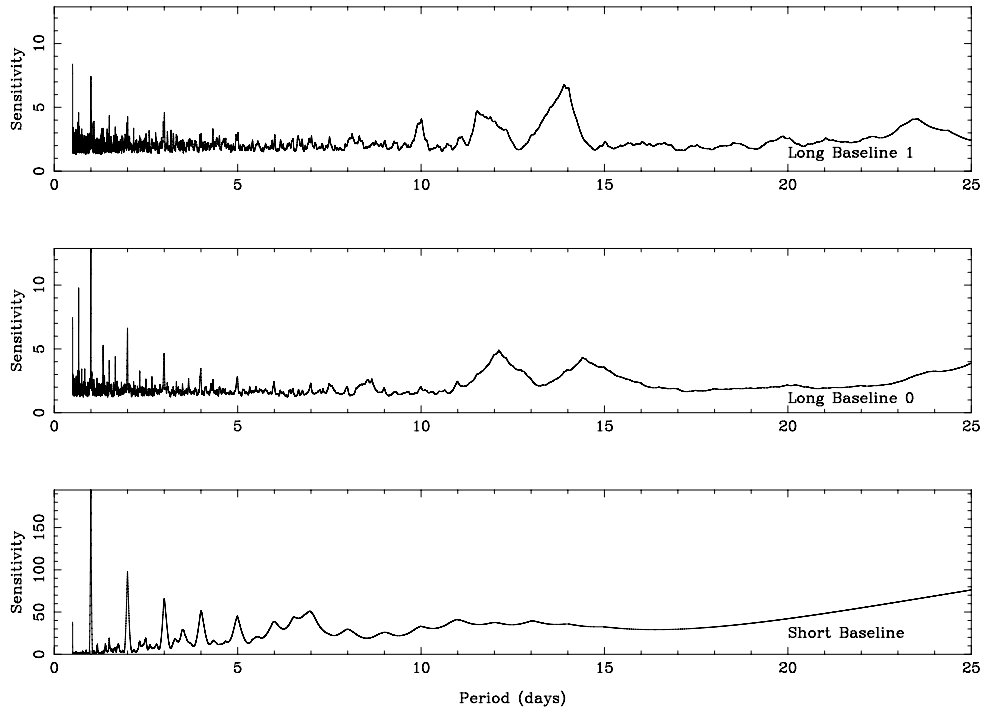


Figure 4. The Saunders statistic, as calculated from a representative light curve from each data set, in which more than 60 per cent of the data points in the light curve were unflagged.

Therefore, we prefer periods from the SB data set for periods less than 7 d.

In Fig. 7, we show the X-ray counts from Getman et al. (2006) for those objects for which we found periods, and for those objects in which no periods were found. Objects with detections in the X-ray catalogue of Getman et al. (2006) were matched with our optical catalogue using a 3-arcsec matching radius. A cut in colour–magnitude space (see Section 3.2) was applied to our optical catalogue to reduce the contamination from foreground objects. The matches were then divided into two groups; those in which we detected periods, and those in which no period was found. We see a suggestion that the stars in which we found periods are significantly more X-ray luminous than those stars for which a period was not found. This result is not formally significant; A 1D K–S test gives a 13 per cent chance that they were drawn from the same parent distribution. Thus it is possible, though not certain, that our catalogue of periodic objects is biased against X-ray faint sources. This bias is presumably introduced because strong star spot activity is associated with increased X-ray emission. Whether this introduces bias into our period distribution remains to be seen. There is no evidence for a correlation between X-ray counts and rotational period *within* the stars for which periods were found.

To summarize; our survey is sensitive even to weak periodic signals below 7 d and down to masses of $0.2 M_{\odot}$. For longer periods, completeness is somewhat lower, and we are, generally speaking, only sensitive to stronger periodic signals ($S/N \geq 5$). Thus, our periodic data set is biased to some degree towards shorter rotational periods.

3.2 Rejection of background and foreground objects

There will also be some contamination of our sample by non-PMS stars. Whilst variability is a very good indicator of youth, periodic variables do exist amongst the field population, and these should

be removed from our sample. The most practical way of removing foreground and background objects is via cuts in colour–magnitude space. PMS objects are larger and correspondingly brighter than main-sequence stars of a given colour and distance. A simple cut in colour–magnitude space can remove a large amount of the contamination by main sequence and other foreground objects. We decided on an appropriate cut by-eye, which is shown in Fig. 8. Of the 704 periodic stars, 553 have unflagged colours placing them above and to the right-hand side of the cut in Fig. 8. Our data set is still not free of possible contamination. Lamm et al. (2004) point out that significant contamination from variable background giants (e.g. RR Lyrae stars) can lie within the PMS region as defined by the cut above, and a further cut is required to remove these objects. Lamm et al. (2004) suggest that the difference in $(R - H\alpha)$ colours between giants and main-sequence or PMS stars allows for rejection based upon this colour index. In addition, the extra reddening experience by background giants gives them larger $(V - I)$ colours than main-sequence or PMS stars. Therefore, following Lamm et al. (2004), we use the $(R - H\alpha)$ versus $(V - I)$ colour–colour diagram, shown in Fig. 9, to reject background giants. The locus of PMS stars was defined as the median $(R - H\alpha)$ colour as a function of $(V - I)$ for all periodic stars which survived our initial cut in V versus $(V - I)$. A quadratic fit to the median defines the PMS locus as

$$(R - H\alpha)_{\text{locus}} = -0.024(V - I)^2 + 0.179(V - I) - 3.126. \quad (1)$$

To reject background giants, we define a lower cut-off, shown in Fig. 9 as a dashed line, by $(R - H\alpha) - 1.65\delta$, where δ is a fit to the standard deviation in $(R - H\alpha)$ as a function of $(V - I)$, given by

$$\delta = \exp[0.66(V - I) - 4.23]. \quad (2)$$

Of the 553 stars which passed our V versus $V - I$ cut, 481 had unflagged colours in both $(R - H\alpha)$ and $(V - I)$, six of which were rejected as background giants. Our final data set thus consists

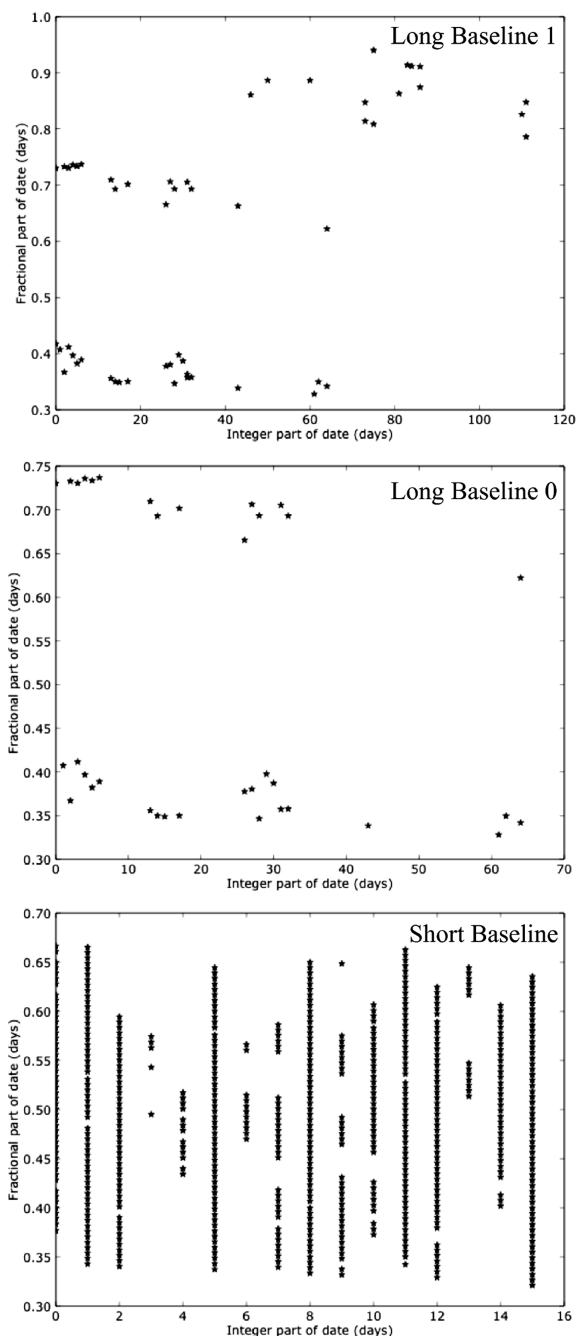


Figure 5. Time sampling of our data sets. The x-axis shows the integer part of the time elapsed since the first observation. The y-axis shows the fractional part of the time elapsed since the first observation.

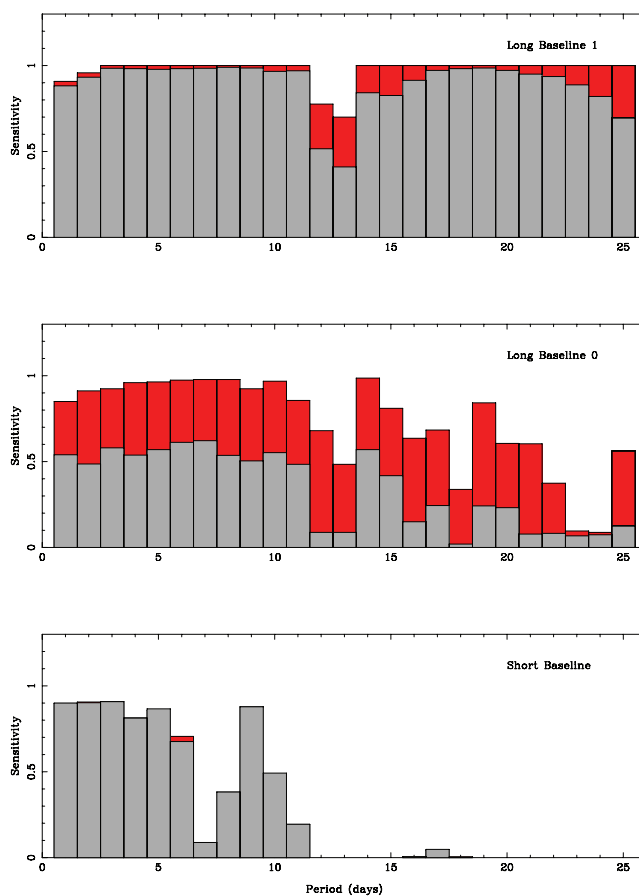


Figure 6. The fraction of correctly recovered periods, as a function of period, for a representative light curve from each data set. The red histogram shows the sensitivity to sinusoidal periods with S/N of 5, the grey histogram shows the sensitivity to sinusoidal periods with S/N of 2.

of 475 periodic variables which are very likely PMS members of the Cep OB3b star-forming region.

4 AGE AND DISTANCE OF CEP OB3B

In Mayne et al. (2007), we derived ages for a group of well studied star-forming regions, including Cep OB3b, based on the fact that the luminosity of the PMS declines with age. Thus, the derived age clearly depends on the distance assumed for each group, which in Mayne et al. (2007) we took from the literature. Realising these literature distances were the major source of uncertainty in the ages, Mayne & Naylor (2008) derived consistent distances with robust uncertainties by fitting the main-sequence stars in each region using

Table 2. Data on the detected periodic variables are available in this format at <http://www.astro.ex.ac.uk/people/timn/Catalogues/tables.html>. This table is a sample only, to indicate the format of the online table (see also Supporting Information). The flag column indicates data quality, and is explained in full at <http://www.astro.ex.ac.uk/people/timn/Catalogues/format.html>.

Field/CCD (field.ccd)	ID	RA (J2000)	Dec. (J2000)	xpos (ccd)	ypos (ccd)	Period	Uncertainty	Flag	MAG	Uncertainty	Flag
1.04	549	22 55 27.231	+62 43 28.87	474.084	2343.941	2.089	0.010	OO	15.119	0.008	OO
1.04	43	22 57 2.094	+62 44 7.04	319.608	374.983	2.630	0.010	OO	15.297	0.008	OO

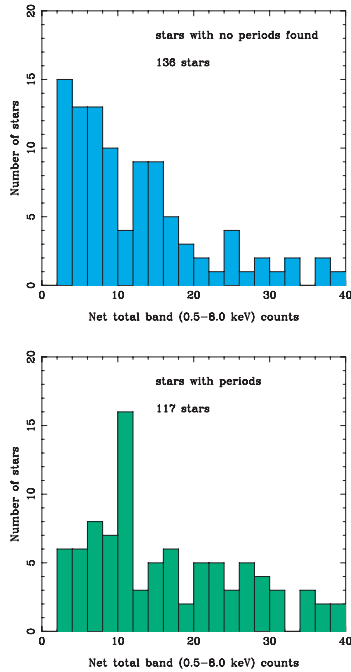


Figure 7. The histogram of X-ray counts for objects with known periods (bottom panel) and for objects with no known periods (top panel). The X-Ray flux of objects for which we found periods is systematically higher than for objects where no period was found.

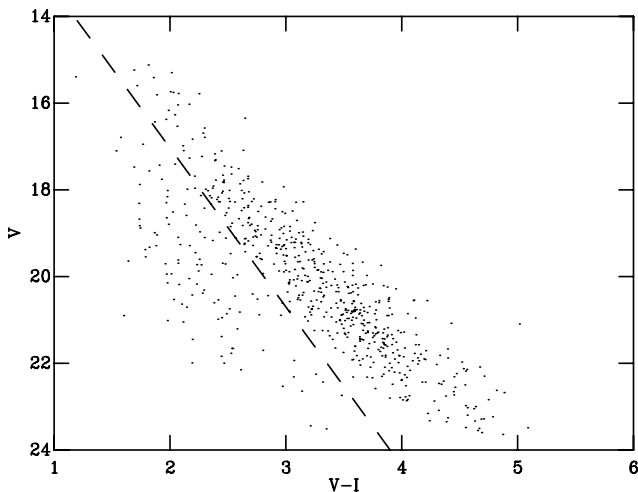


Figure 8. The CMD of periodic variables in Cep OB3b. An initial colour cut, used to select PMS objects is plotted with a dashed line.

the τ^2 method of Naylor & Jeffries (2006). We have applied the same methods to the γ Vel association and Vel OB2 (Jeffries et al. 2009) and NCC 2169 (Jeffries et al. 2007), which along with the regions presented in Mayne & Naylor (2008) represent a self-consistent set of ages and distances for a significant group of young clusters and star-forming regions.

Clearly, we must attempt to fit Cep OB3b into this system, but although we attempted this in Mayne & Naylor (2008), we failed to do so because we had only a few stars which could be used for main-sequence fitting, and they gave an answer sharply at variance with the literature values. In what follows, we use the stars from Cep OB3a as well as Cep OB3b, and still obtain an answer which is different from that determined by others, but we now understand

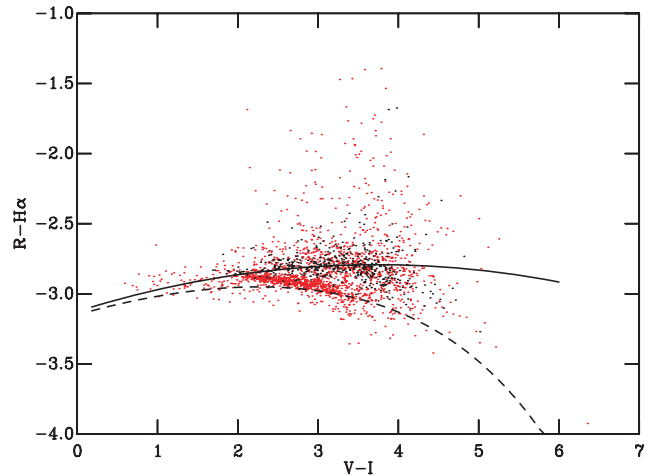


Figure 9. The $(R - H\alpha)$ versus $(V - I)$ colour-colour diagram for Cep OB3b. The red (light grey) points represent all the stars for which we have photometry. The black dots are those periodic stars which survived the cut in the V versus $V - I$ CMD. The PMS locus is plotted as a solid line, and the locus used to reject background giants is plotted as a dotted line.

that the difference is due to the earlier work using a Schmidt-Kaler (1982) main sequence (as opposed to his zero-age main sequence), which is significantly brighter than more modern work.

To determine an age in the same way as Mayne et al. (2007), we must place the PMS of Cep OB3b in a V_0 versus $(V - I)_0$ colour-magnitude diagram (CMD), and compare it with similar sequences for other star-forming regions. If we carry out such a comparison by plotting the members of each group in a CMD the number and spread of the data points make the plot impossible to interpret. Instead, as described in Mayne et al. (2007), we use splines fitted through the members. To place Cep OB3b in such a diagram we need the apparent distance modulus (to correct V), and $E(V - I)$ to correct $V - I$. In what follows, we derive these by dereddening and then fitting the main sequence, in an identical fashion to Mayne & Naylor (2008).

4.1 MS star individual reddenings and extinctions

Pozzo (2001) provided a list of members of both subgroups with photometry in Blaauw, Hiltner & Johnson (1959, hereafter BHJ).² We dereddened each of these in $U - B$ versus $B - V$ and used the implied extinction in V to create the CMD shown in Fig. 10. To do this, we have used the extinction vectors of Bessell, Castelli & Plez (1998), and a Geneva-Bessell main sequence (see Bessell et al. 1998; Lejeune & Schaerer 2001; Mayne & Naylor 2008). The mean extinction of the sample is $E(B - V) = 0.79$ with an rms of 0.16 mag.

4.2 True distance modulus

For our distance modulus determination, we must ensure we fit only those stars which are on the main sequence (see the discussion in Mayne & Naylor 2008). The bright limit to the main sequence is defined by the turn-off, which becomes fainter with age. In Fig. 10, we show the 3 and 10 Myr isochrones, which make it clear that the

² The star numbers in BHJ for these are as follows. Subgroup (a): 14, 18, 19, 23, 37, 44, 46, 47, 50, 54, 56, 59, 66, 68, 69, 70, 75, 76 and 77. Subgroup (b): 2, 8, 10, 11, 15, 16, 17, 20, 22, 24, 25, 26, 31, 33, 39, 40 and 41.

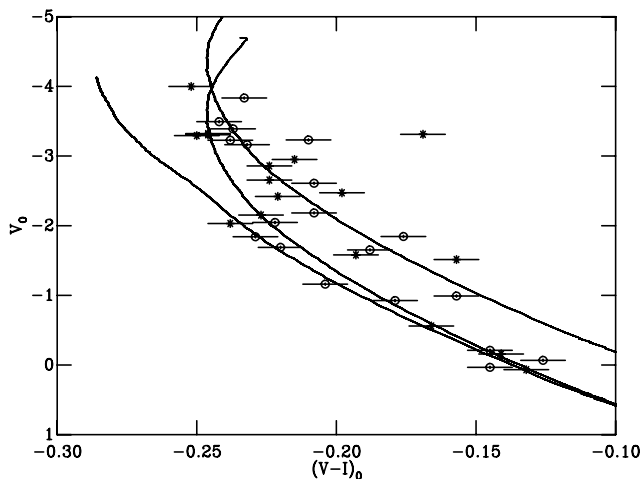


Figure 10. The members of Cep OB3a (circles with error bars) and Cep OB3b (stars with error bars). The photometry (from BHJ), and the colours have then been dereddened and the magnitude corrected for extinction by deriving colour excesses in the $U - B$ versus $B - V$ plane. The magnitudes have been converted into absolute magnitudes using the best-fitting distance modulus of 8.8. The curves are Geneva–Bessell isochrones for (from faintest to brightest) 3, 10 and 3 Myr equal-mass binary sequence.

turn-off is not a sharp transition. We chose these ages as 3 Myr is the youngest age available in the Geneva isochrones, whilst it is unlikely that any members of Cep OB3 are older than 10 Myr. We therefore fit only those stars lying below $V_o = -1.5$, since brighter than this the two sequences separate by more than 0.009 mag in $B - V$, corresponding to half the uncertainty for the photometry quoted by BHJ. The faint end of the main sequence, within the CMD, is approximately defined by the radiative-convective (RC) gap, which is only defined (and observable) for clusters younger than 20 Myr old (Mayne et al. 2007). Although some stars blueward of the RC gap will not have reached the main sequence, their position in CMD space is very close to the main-sequence locus at these ages (see discussion in Mayne & Naylor 2008). Even at the age of the ONC (2 Myr) the stars bluer than $B - V = 0$ are on the main sequence, so the entire remaining sample can be fitted.

We can now fit a main-sequence isochrone to the remaining data in Fig. 10, using the τ^2 fitting procedure described in Mayne & Naylor (2008), with the improvements in Naylor (2009). Using the Geneva–Bessell isochrones we obtain the fit shown in Fig. 11, and a true distance modulus of 8.8 ± 0.2 mag.

4.3 Apparent V-band distance modulus

Since our aim is to correct the PMS data of Mayne et al. (2007) into the V_o versus $(V - I)_o$ CMD, we need the apparent distance modulus for the field from which those data were taken. This is the same INT field as observed here, within which there are 12 BHJ stars, which give a mean $E(B - V) = 0.83 \pm 0.11$ where the quoted uncertainty is the rms about the mean. We can then calculate A_V as $3.26 \times 0.83 = 2.71$, and the apparent V-band distance modulus as $8.8 + 2.7 = 11.5 \pm 0.2$. This is independent of any assumptions about $R = A_V/[E(B - V)]$, since changing R changes the extinction-free magnitudes of Fig. 10, and hence the true distance modulus by an equal and opposite amount to the change in V-band extinction.

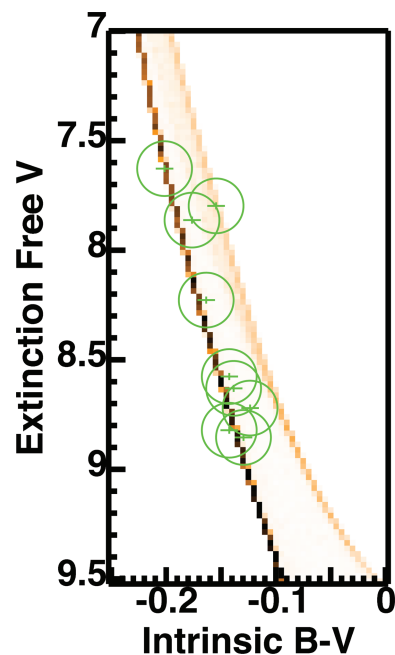


Figure 11. The fit to the main-sequence data. The data are shown as circled error bars, and the colour scale is the best-fitting model (ρ in equation 3 of Naylor & Jeffries 2006).

4.4 Reddening in $V - I$

Finally, we need $E(V - I)$ to correct $V - I$. The usual way of proceeding at this point would be to use the ratio $E(V - I)/E(B - V)$ to calculate $E(V - I)$ from $E(B - V)$. But in this case there is a subtle issue which must be addressed. For a given column of interstellar material between the observer and a star the extinction (e.g. A_V) and reddenings [e.g. $E(B - V)$] depend on the colour of the star being observed. Therefore to specify the column density precisely, one must specify the colour of the star for which the measurement was made. For B-stars let us refer to $E(B - V)_B$, and for the red PMS stars $E(B - V)_R$. To construct the normal colour dependent reddening vectors one constructs a continuous sequence of ratios from say $E(V - I)_B/E(B - V)_B$ to $E(V - I)_R/E(B - V)_R$. Our case is somewhat different, we have measured $E(B - V)_B$ but wish to know $E(V - I)_R$, and therefore need the ratio $E(V - I)_R/E(B - V)_B$. This can be obtained folding a blue stellar atmosphere through the appropriate filter responses, and then applying a given column density to the flux, to obtain $E(B - V)_B$. Using the same column density, one can also obtain $E(V - I)_R$. Whilst Bessell et al. (1998a) find that $E(V - I)_R/E(B - V)_R = 1.44$ for $(V - I)_0 = 2$, we find that with identical atmospheres and the extinction law of Cardelli, Clayton & Mathis (1989) $E(V - I)_R/E(B - V)_B = 1.26$ for red stars of $(V - I)_0$ of approximately two.

In principle, A_V should show a similar effect, with red stars being less affected by a given column density than blue ones, and so, in principle we have overestimated the V-band extinction for the red stars. However, we have calculated this effect, and find it is less than 0.03 mag, and so ignore it. Thus, our final estimate of $E(V - I)$ for appropriate stars of PMS colours is $1.26 \times 0.83 = 1.05$.

4.5 Age estimate

Now, we have distance moduli we can obtain a relative age for Cep OB3b by comparing the absolute magnitude of its PMS with

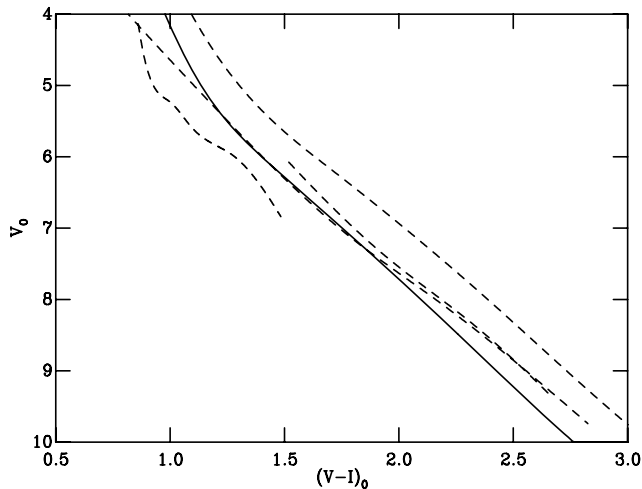


Figure 12. A comparison of the position of the PMS in a CMD of Cep OB3b with other young groups. The solid curve is for Cep OB3b. The dashed curves are the sequences for (from left- to right-hand side) the ONC (2 Myr), NGC 2362 (lower, 4–5 Myr), IC348 (upper 4–5 Myr) and h and χ Per (13 Myr).

those of other young groups. Within any young (<5 Myr) OB association or cluster, there is a large scatter in the luminosity of the PMS members at any given colour (for a discussion of this see, for example, Burningham et al. 2005, and references therein). To make the comparison between groups easier, therefore, we fit a curve through the members of each group, and then compare the positions of these fits in an absolute-magnitude intrinsic-colour diagram. The fits are taken from Mayne et al. (2007) and were constructed by binning the data by magnitude, finding the median magnitude and colour within each bin, and then fitting a spline through the resulting points. The corrections to absolute magnitude and intrinsic colour were taken from either Mayne et al. (2007) or Mayne & Naylor (2008), except for Cep OB3b for which we used the values derived above. The result is shown in Fig. 12, which shows the position of Cep OB3b very closely matches that of IC348 and NGC 2362, both which were assigned ages of 4–5 Myr, and so we will use an age of 4.5 Myr for Cep OB3b throughout this paper

4.6 Comparison with literature values

In Mayne et al. (2007), we adopted an age of about 3 Myr, and a distance modulus of 9.65 ± 0.2 mag. Our revised true distance modulus of 8.8 mag is much lower, yet our new age is only slightly older. The Mayne et al. (2007) distance was essentially the one derived by Moreno-Corral et al. (1993), which relies on the Schmidt-Kaler (1982) main sequence for stars around the solar neighbourhood. This is about 0.8 mag brighter in M_V than the Geneva–Bessell isochrone for 3 Myr, and indeed the *zero-age* Schmidt-Kaler (1982) main sequence. This effect alone would push Cep OB3b to an age of around 10 Myr, but is partially compensated for by our value of $E(V - I)/E(B - V)$. The difference between the value we use, and say that of Bessell et al. (1998), results in shift of 0.15 mag in $V - I$, decreasing the age from 10 Myr to the 4.5 Myr adopted here.

Given the significant change in the distance compared with literature values, and the low value of the $V - I$ colour excess we have used, we have checked that the resulting age is consistent with other available age indicators. These are as follows.

(i) Cep OB3b has a large RC gap (see Mayne et al. 2007) suggesting an age of around 3 Myr.

(ii) The PMS shows a large ‘age spread’ in the CMD, which Mayne et al. (2007) show is characteristic of groups younger than about 5 Myr.

(iii) The turn-off age derived by Jordi, Trullols & Galadí-Enriquez (1996) is 5.5 Myr, and although revised distance modulus would make this slightly younger, the turn-off and PMS ages are clearly not grossly discrepant.

(iv) There is still molecular material around the group (it is obvious in the optical images and the extinction is patchy), which is again normally associated with young groups. Thus, we conclude that all current age estimates are in concordance.

5 PERIOD DISTRIBUTION

5.1 Mass dependence of rotation

The dependence of rotation period upon mass was first shown for the ONC by Herbst et al. (2002), and later confirmed in NGC 2264 (Lamm et al. 2004, 2005) and IC 348 (Littlefair et al. 2005). In general, lower mass stars rotate significantly faster than higher mass stars, both in the PMS phase and in young clusters (e.g. Scholz et al. 2005; Herbst et al. 2007; Scholz, Eislöffel & Mundt 2009). The reasons for this are not yet clear, though hints are emerging that it is related to a change in magnetic structure with mass (Scholz et al. 2009; Donati et al. 2010).

We calculated masses for our stars by comparing extinction and distance corrected I -band magnitudes with the 4.5 Myr isochrones of Baraffe et al. (1998). For this, we need the apparent distance modulus in I , which we calculate from the true distance modulus (Section 4.2) and A_I . We do this using the ratio $A_I/E(B - V)_B$, calculated for red stars in the same way as described in Section 4.4. We find this ratio is 1.94 (cf. 1.89 from Bessell et al. 1998), giving an apparent I -band distance modulus for Cep OB3b of 10.4. We also calculated masses for the periodic stars in NGC 2264 and 2362. We adopted ages, true distance moduli and $E(B - V)_B$ from Mayne & Naylor (2008). A_I is calculated as outlined above to obtain the apparent distance modulus in I , and the masses are derived by comparison with the same Baraffe et al. (1998) isochrones at the appropriate age. For the ONC a similar method was used, except that individual dereddened I -band magnitudes of Hillenbrand (1997) were used. In this way, we have ensured that all clusters have masses and ages which are determined in a self-consistent manner. The results are shown in Fig. 13, which shows the rotation periods of young stars in Cep OB3b, NGC 2362, 2264 and the ONC, plotted as a function of mass.

We can see from Fig. 13 that in many young clusters there is a strong dependence of rotation with mass, in the sense that the stars with masses below $0.4 M_\odot$ show a dearth of slow rotators. This can readily be seen in the period distributions of NGC 2264 and 2362, for example. To study this effect in Cep OB3b, we divide our data into high- and low-mass samples. The high-mass sample contains stars with masses between 1.0 and $0.4 M_\odot$, whilst the low-mass sample contains stars with masses between 0.4 and $0.2 M_\odot$. The rotation distribution in Cep OB3b supports the general picture seen in other clusters; the low-mass stars are rotating, on average, more rapidly than the higher mass stars. The median period of the low-mass stars is 3.7 d, against 4.4 d for the high-mass stars. Unlike in other clusters, however, this result is barely statistically significant. A 1D K–S test gives a 6 per cent chance that the low- and high-mass stars were drawn from the same period distribution. Under

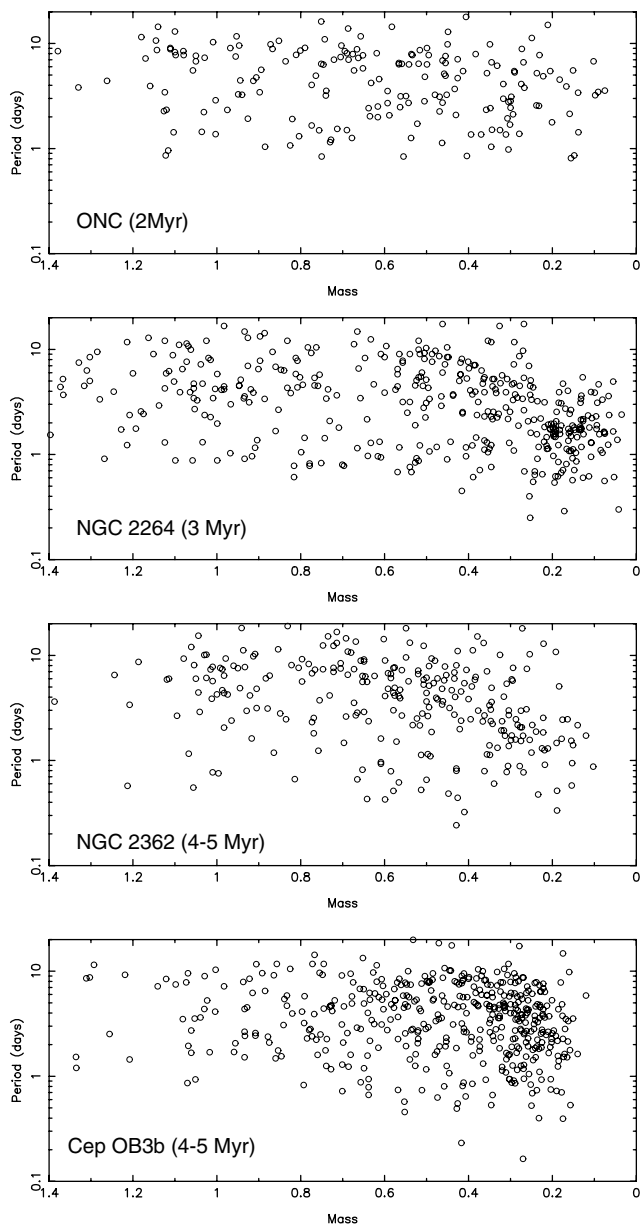


Figure 13. Rotation period plotted against mass for the stars in Cep OB3b, as well as for other clusters with large collections of rotation data within the literature. Rotation periods were taken from Herbst et al. (2002) (ONC), Lamm et al. (2004), Lamm et al. (2005) (NGC 2264) and Irwin et al. (2008) (NGC 2362). See text for details of how masses were assigned.

the assumption that the period distributions in high- and low-mass stars differ only in their median value, a Mann–Whitney test gives a 3 per cent chance that the median period is the same for the high- and low-mass stars in Cep OB3b. The difference is much more marked in other clusters; the same K–S test on the NGC 2362 sample gives a probability of less than 0.01 per cent that the high- and low-mass stars were drawn from the same distribution. Thus, whilst the stars in Cepheus show the same mass dependence of rotation seen elsewhere, the difference is less marked than is seen in other clusters.

5.1.1 Comparison with NGC 2362

It is apparent that the low-mass stars in Cep OB3b are rotating more slowly than those in other clusters. A comparison with NGC 2362 is most interesting, as it is at a similar age to Cep OB3b. The median period for low-mass stars in Cep OB3b is 3.7 d, compared to 2.3 d for NGC 2362. A 1D K–S test gives a 0.1 per cent chance that the periods of low-mass stars in the two clusters were drawn from the same period distribution. Amongst the high-mass stars the picture is different, with the high-mass stars in Cep OB3b rotating more rapidly than their counterparts in NGC 2362. The median period for the high-mass stars in Cep OB3b is 4.4 d, compared to 4.9 d for NGC 2362. This difference is only weakly significant though; a 1D K–S test gives a 6 per cent chance that the periods of high-mass stars in the two clusters were drawn from the same period distribution. It is not clear why the two clusters should be so different. Our simulations (see Section 3.1) suggest that we should have found almost all periods below 7 d with amplitudes greater than 0.02 mag in stars down to $0.2 M_{\odot}$. Similar calculations by Irwin et al. (2008) suggest that the survey in NGC 2362 was sensitive to periods of up to 10 d, with the same amplitude and for stars of the same mass. Thus, biases could potentially have explained an deficit of slow rotators in Cep OB3b, but not an excess.

Another possibility is contamination of our periodic sample. We have taken steps to remove foreground and background contamination from our sample (see Section 3.2), but it remains possible that there is contamination from a second population of PMS stars towards Cep OB3b. This second population need not share the distance and age of the main population, so masses assigned to its members would be in error. In this way slowly rotating, high-mass PMS stars might be confused for lower mass objects. Optical spectroscopy of the region could test this possibility. If systematic error is not responsible for the observed difference between Cep OB3b and NGC 2362, it follows that different clusters at similar ages can show very different rotation distributions. This is not the first time such environmental differences have been found; the young stars in IC348 rotate much slower than those in the similarly aged NGC 2264 (Littlefair et al. 2005).

5.2 Rotation period and H α emission

In order to gauge the effect of accretion upon rotation rate, we examine here the link between rotation period and H α emission. Other authors (e.g. Rebull et al. 2005; Cieza & Baliber 2007) have examined the link between mid-IR excess and rotation. Whilst an infrared excess is good evidence for a disc it is not evidence for ongoing accretion, which is necessary for angular momentum regulation. H α emission, on the other hand, is a signature of ongoing accretion, and might also be expected to correlate with rotation rate. Indeed, Lamm et al. (2005) show that there is such a correlation in NGC 2264, in the sense that the stars showing strong H α emission rotate more slowly, as a group, than those lacking H α emission. A word of caution is needed: H α emission strength is only an indicator of *current* accretion rate. Since the star-disc interaction, or a stellar wind, can only remove angular momentum on a finite time-scale, it would be more meaningful to compare rotation rate against the *time-averaged* accretion rate, taken over a comparable time-scale. Additionally, it should always be born in mind that photometric monitoring can in principle be biased against the detection of periods in strongly accreting stars, although Littlefair et al. (2005) showed that dense temporal sampling, as used in this paper, is effective in reducing such a bias.

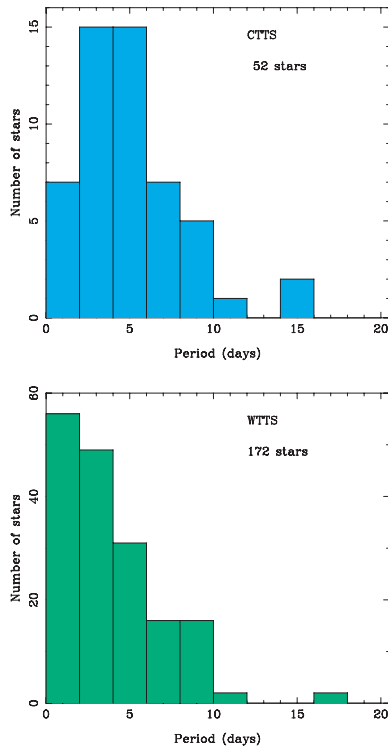


Figure 14. Period distributions for Cep OB3b, divided into samples according to $H\alpha$ strength. The stars are grouped in accreting, CTTS and non-accreting, WTTS. See text for details of how stars were divided into these samples.

We divide our sample into accreting and non-accreting objects in the $V - I$, $R - H\alpha$ diagram, following Lamm et al. (2004). Weak-line T-Tauri stars (WTTS) are assumed to be non-accreting, and are defined in this paper as objects with little or no $H\alpha$ emission, as defined by

$$(R - H\alpha) - (R - H\alpha)_{\text{locus}} + \Delta(R - H\alpha) < 0.0, \quad (3)$$

where $(R - H\alpha)_{\text{locus}}$ is defined by equation (1). Classical T-Tauri stars (CTTS) are objects with strong $H\alpha$ emission, and are assumed to be accreting. In this paper, we define CTTS as those objects which satisfy

$$(R - H\alpha) - (R - H\alpha)_{\text{locus}} - \Delta(R - H\alpha) > 0.1. \quad (4)$$

Lamm et al. (2005) show that equation (4) corresponds roughly to $W_\lambda(H\alpha) > 10 \text{ \AA}$, which is frequently used to select CTTS, based on the equivalent width of $H\alpha$.

We find evidence that accretion is influencing rotation in Cep OB3b. The CTTS are rotating more slowly on average than the WTTS (see Fig. 14). This difference is statistically significant; a 1D K-S test gives a 5 per cent chance they were drawn from the same parent distribution. Thus, the data in Cepheus lend some support to the generally accepted picture that accretion discs play a significant role in regulating the angular momentum of young stars. The result is only just statistically significant, however, and a statistically significant difference between CTTS and WTTS is no longer present if the data are broken down into high- and low-mass subsamples. This is perhaps not surprising. Our method of dividing stars into CTTS and WTTS is rather crude, relying as it does on narrow-band photometry, rather than spectroscopy; it is not without sensitivity biases which can be a function of mass. Also, we classify relatively a few objects as CTTS, which reduces the statistical power of our

sample. To test the influence of present-day accretion on rotation periods, good quality $H\alpha$ spectroscopy of our periodic objects is highly desirable.

6 DISCUSSION

Our results show that Cep OB3b is a rich cluster for studying the evolution of stellar angular momentum. The periodic data in Cep OB3b broadly confirm the general picture of angular momentum evolution in young stars; accreting objects are rotating more slowly than non-accretors, confirming the influence of discs on the angular momentum of young stars. As seen in other young clusters, the low-mass stars are rotating more rapidly than the high-mass stars, but this mass dependence is much weaker than that typically observed. Compared to the similarly aged cluster NGC 2362, Cep OB3b has very slowly rotating low-mass stars, and possibly an excess of fast rotators amongst the high-mass stars. There remains a possibility that this difference between the two clusters is a systematic error, perhaps related to contamination within our periodic data base by a second PMS population. Optical spectroscopy of the region can test for this systematic effect, and can also improve our mass determinations, by determining individual extinction values for our periodic stars.

If this difference between the two clusters is not systematic in origin, it confirms the findings of Littlefair et al. (2005), that clusters of similar ages can show very different rotational period distributions. Such environmental differences could possibly arise as a result of differing angular momentum budgets between clusters or they might reflect differences in disc lifetimes between star-forming regions. These results should act as a cautionary tale for models which aim to reproduce the angular momentum evolution of stars (e.g. Herbst et al. 2002; Irwin et al. 2007). These models are based on the assumption that the rotation period distributions of different clusters can be assembled into an evolutionary sequence, but this assumption is broken if environmental differences between the clusters play a larger role than evolutionary effects, due to magnetic wind braking, disc locking or contraction towards the main sequence. It is thus important to fit such models to data sets which include rotation periods from more than one cluster at each age, to gauge the impacts of environmental differences between clusters.

7 CONCLUSIONS

We present a photometric study of I -band variability towards the young association Cep OB3b. The study is sensitive to periodic variability on time-scales of less than a day, to more than 20 d. The result is a data base of 704 periodic variables in the field of Cep OB3b. A random inspection of 200 of these objects suggests that around 97 per cent of these periods are genuine. Colour cuts using V , I , R and narrow-band $H\alpha$ photometry are used to reject contaminating objects, leaving 475 objects with measured rotation periods, which are very likely PMS members of the Cep OB3b star-forming region.

We revise the distance and age to Cep OB3b, putting it on the consistent age and distance ladder of Mayne & Naylor (2008). This yields a distance modulus of 8.8 ± 0.2 mag, corresponding to a distance of 580 ± 60 pc, and an age of 4–5 Myr. For the purposes of this paper, we therefore adopt an age of 4.5 Myr.

The rotation period distribution confirms the general picture of rotational evolution in young stars, exhibiting both the correlation between accretion and rotation expected from disc locking, and the dependence of rotation upon mass that is seen in other star-forming

regions. However, this mass dependence is much weaker than seen in other regions. Comparison to the similarly aged NGC 2362 shows that the low-mass stars in Cep OB3b are rotating much more slowly. This points to a possible link between star-forming environment and rotation properties. Such a link would call into question models of stellar angular momentum evolution, which assume that associations can be assembled into an evolutionary sequence, thus ignoring environmental effects.

ACKNOWLEDGMENTS

SPL is supported by an RCUK fellowship. This research has made use of NASA's Astrophysics Data System Bibliographic Services. Based on observations made with the INT operated on the island of La Palma by the Isaac Newton Group in the Spanish Observatorio del Roque de los Muchachos of the Instituto de Astrofísica de Canarias. We thank the many INT observers who performed the observations which constitute the LB0 data set for us. The Faulkes Telescope Project is an educational and research arm of the Las Cumbres Observatory Global Telescope Network (LCOGTN).

REFERENCES

- Baraffe I., Chabrier G., Allard F., Hauschildt P. H., 1998, *A&A*, 337, 403
 Bessell M. S., Castelli F., Plez B., 1998, *A&A*, 333, 231
 Bessolaz N., Zanni C., Ferreira J., Keppens R., Bouvier J., 2008, *A&A*, 478, 155
 Blaauw A., Hiltner W. A., Johnson H. L., 1959, *ApJ*, 130, 69 (BHJ)
 Bouvier J., Alencar S. H. P., Harries T. J., Johns-Krull C. M., Romanova M. M., 2007, in Reipurth B., Jewitt D., Keil K., eds, *Protostars and Planets V Magnetospheric Accretion in Classical T Tauri Stars*. Univ. of Arizona Press, Tucson, p. 479
 Burningham B., Naylor T., Littlefair S. P., Jeffries R. D., 2005, *MNRAS*, 363, 1389
 Cardelli J. A., Clayton G. C., Mathis J. S., 1989, *ApJ*, 345, 245
 Cieza L., Baliber N., 2007, *ApJ*, 671, 605
 Donati J. et al., 2010, *MNRAS*, 402, 1426
 Fendt C., 2007, in Bouvier J., Appenzeller I., eds, *Proc. IAU Symp. 243, Star-Disk Interaction in Young Stars*. Cambridge Univ. Press, Cambridge, p. 265
 Getman K. V., Feigelson E. D., Townsley L., Broos P., Garmire G., Tsujimoto M., 2006, *ApJS*, 163, 306
 Herbst W. et al., 2002, *PASP*, 114, 1167
 Herbst W., Eisloffel J., Mundt R., Scholz A., 2007, in Reipurth B., Jewitt D., Keil K., eds, *Protostars and Planets V The Rotation of Young Low-Mass Stars and Brown Dwarfs*. Univ. of Arizona Press, Tucson, p. 297
 Hillenbrand L. A., 1997, *AJ*, 113, 1733
 Horne J. H., Baliunas S. L., 1986, *ApJ*, 302, 757
 Irwin J., Hodgkin S., Aigrain S., Hebb L., Bouvier J., Clarke C., Moraux E., Bramich D. M., 2007, *MNRAS*, 377, 741
 Irwin J., Hodgkin S., Aigrain S., Bouvier J., Hebb L., Irwin M., Moraux E., 2008, *MNRAS*, 384, 675
 Jeffries R. D., Oliveira J. M., Naylor T., Mayne N. J., Littlefair S. P., 2007, *MNRAS*, 376, 580
 Jeffries R. D., Naylor T., Walter F. M., Pozzo M. P., Devey C. R., 2009, *MNRAS*, 393, 538
 Jordi C., Trullols E., Galadi-Enriquez D., 1996, *A&A*, 312, 499
 Koenigl A., 1991, *ApJ*, 370, L39
 Lamm M. H., Bailer-Jones C. A. L., Mundt R., Herbst W., Scholz A., 2004, *A&A*, 417, 557
 Lamm M. H., Mundt R., Bailer-Jones C. A. L., Herbst W., 2005, *A&A*, 430, 1005
 Lejeune T., Schaerer D., 2001, *A&A*, 366, 538
 Linnell Nemeč A. F., Nemeč J. M., 1985, *AJ*, 90, 2317
 Littlefair S. P., Naylor T., Burningham B., Jeffries R. D., 2005, *MNRAS*, 358, 341
 Long M., Romanova M. M., Lovelace R. V. E., 2005, *ApJ*, 634, 1214
 Matt S., Pudritz R. E., 2008, *ApJ*, 681, 391
 Mayne N. J., Naylor T., 2008, *MNRAS*, 386, 261
 Mayne N. J., Naylor T., Littlefair S. P., Saunders E. S., Jeffries R. D., 2007, *MNRAS*, 375, 1220
 Moreno-Corral M. A., Chavarría K. C., de Lara E., Wagner S., 1993, *A&A*, 273, 619
 Naylor T., 2009, *MNRAS*, 399, 432
 Naylor T., Jeffries R. D., 2006, *MNRAS*, 373, 1251
 Naylor T., Totten E. J., Jeffries R. D., Pozzo M., Devey C. R., Thompson S. A., 2002, *MNRAS*, 335, 291
 Pozzo M., 2001, PhD thesis, Keele Univ.
 Pozzo M., Naylor T., Jeffries R. D., Drew J. E., 2003, *MNRAS*, 341, 805
 Rebull L. M., Stauffer J. R., Megeath T., Hora J., Hartmann L., 2005, *BAAS*, 207, 185
 Romanova M. M., Kulkarni A. K., Lovelace R. V. E., 2007, preprint (ArXiv e-prints)
 Saunders E. S., Naylor T., Allan A., 2006, *Astron. Nachrichten*, 327, 783
 Schmidt-Kaler T., 1982, *Landolt-Börnstein Vol. VI/2B, Numerical Data and Functional Relationships in Science and Technology*. Springer-Verlag, Heidelberg, p. 14
 Scholz A., Jayawardhana R., Eisloffel J., Froebrich D., 2005, *Astron. Nachrichten*, 326, 895
 Scholz A., Eisloffel J., Mundt R., 2009, *MNRAS*, 400, 1548
 Shu F., Najita J., Ostriker E., Wilkin F., Ruden S., Lizano S., 1994, *ApJ*, 429, 781
 Stassun K. G., Mathieu R. D., Mazeh T., Vrba F. J., 1999, *AJ*, 117, 2941

SUPPORTING INFORMATION

Additional Supporting Information may be found in the online version of this article:

Table 1. Photometry for the INT WFC field observed.

Table 2. Data on the detected periodic variables.

Please note: Wiley-Blackwell are not responsible for the content or functionality of any supporting materials supplied by the authors. Any queries (other than missing material) should be directed to the corresponding author for the article.

This paper has been typeset from a $\text{\TeX}/\text{\LaTeX}$ file prepared by the author.